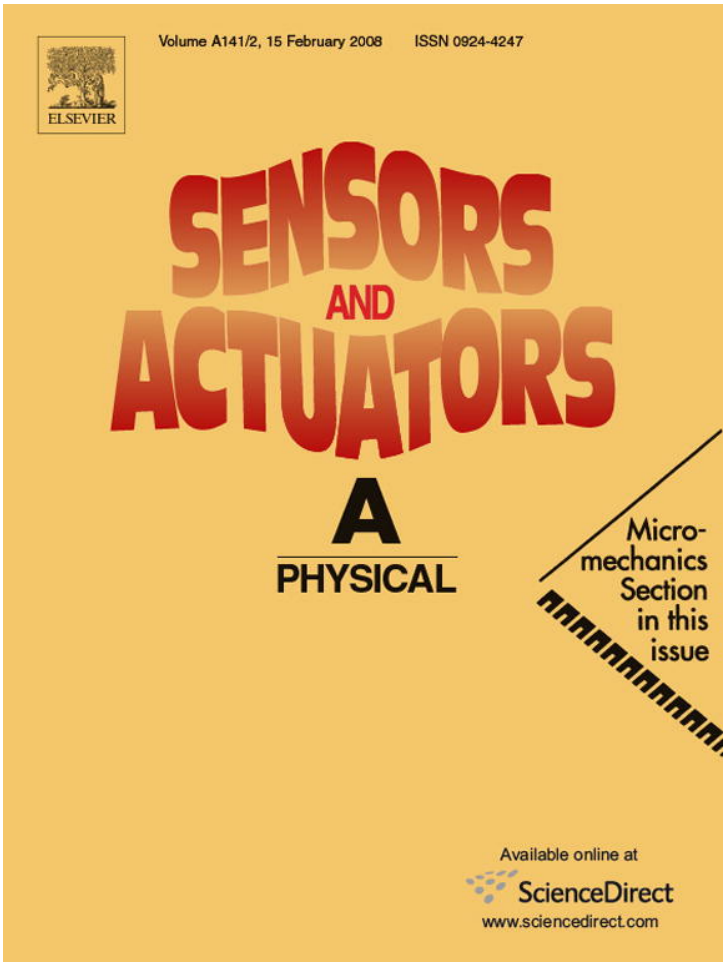

Available online at www.sciencedirect.com
ScienceDirect
Sensors and Actuators A 141 (2008) 523–529
SENSORS AND ACTUATORS A PHYSICAL
www.elsevier.com/locate/sna

A closed-form approach for frequency tunable comb resonators with curved finger contour

Ki Bang Lee [a,*], Liwei Lin [b], Young-Ho Cho [c,d]

[a] KB Lab, 7 Rosewood Drive #10-13, Singapore 737937, Singapore
[b] Berkeley Sensor and Actuator Center, Department of Mechanical Engineering, University of California at Berkeley, USA
[c] Digital Nanolocomotion Center, BioSystems Department, Korea Advanced Institute of Science and Technology, Daejeon, Republic of Korea
[d] Digital Nanolocomotion Center, Mechanical Engineering Department, Korea Advanced Institute of Science and Technology, Daejeon, Republic of Korea

Received 2 January 2007; received in revised form 5 August 2007; accepted 3 October 2007
Available online 9 October 2007

Abstract

Frequency tunable comb resonators have been successfully designed and demonstrated based on a closed-form approach of a curved comb finger contour. Experimentally, the resonant frequency of a laterally driven comb resonator with 186 pairs of curved finger contour has been reduced by 55% from the initial frequency of 19 kHz under a bias voltage of 150 V. The corresponding effective stiffness has been decreased by 80% from the initial value of 2.64 N/m. This closed-form design approach could be extended to microsystems based on electrostatic comb-shape structures such as microaccelerometers, microgyroscopes, and micromechanical filters.

Keywords: Tunable resonator; Electrostatic force; Frequency tuning; Stiffness tuning; Microresonator; Surface micromachining; MEMS

1. Introduction

Microresonant structures have been utilized in various microsystems and various design approaches have been refined and optimized in recent years. For example, piezoelectric materials such as quartz have been employed in magnetic resonance imaging (MRI) and communication systems [1]; solid-state resonant gyroscopes have been applied for angular rate detection [2]; and resonant frequency shifts of microstructures have been used to detect tensile force [3,4]. Among these examples, adjustable capacitance [1] and tuning forks [2–4] are key elements in the design process to control or detect the resonant frequency of the structure. Electrostatic comb structures have been the key design elements for many microstructures including commercial products such as microaccelerometers and gyroscopes. However, for devices based on resonance of microstructures, post-fabrication frequency tuning is generally required to achieve performance uniformity and sensitivity. Previously, various frequency tuning methods have been applied and demonstrated such as: (1) using a control voltage for triangular electrostatic comb arrays for 3% reduction in the resonant frequency [5]; (2) adding material deposition to the mass for 1.2% frequency reduction [6]; (3) thermally expanding microstructures for 50% increase in the resonant frequency under vacuum [7]; and thermal stressing to reduce the resonant frequency of 6.5% [8]. These tuning methods provide small change in resonant frequency [5,6,8] or require high power for frequency tuning operations [7,8].

To achieve wide frequency tuning with low power consumption, researchers have focused on various comb finger designs [9,10]. Both numerical analysis including polynomial fitting technique and boundary element method (BEM) have been used to solve electric field around fixed and movable comb fingers [9] to obtain optimal shape of fingers for linear electrostatic force. Similar optimal design procedures [10] using numerical methods have been used to obtain the linear restoring force for comb actuators.

This paper presents a closed-form design approach for comb finger profiles to achieve constant electrostatic stiffness or linear

* Corresponding author.
E-mail addresses: kblee@kblab.biz, kibanglee@hotmail.com (K.B. Lee).

0924-4247/$ – see front matter © 2007 Elsevier B.V. All rights reserved.
doi:10.1016/j.sna.2007.10.004

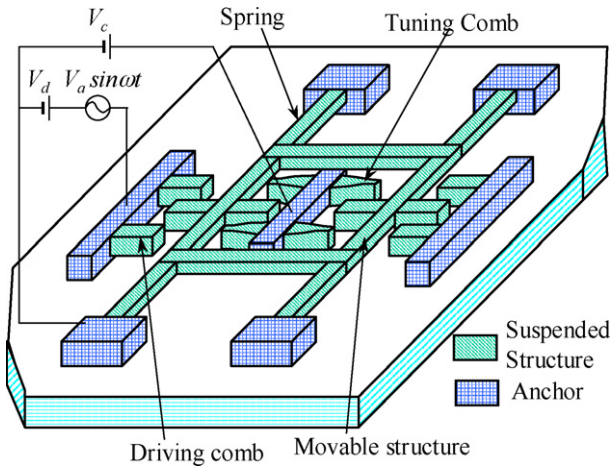

Fig. 1. A tunable microactuator with curved comb-width design: the control voltage, V_c, adjusts the resonant frequency of the microactuator, while the ac and dc voltages actuate the microstructure in the lateral direction.

electrostatic force for comb-shape actuators with experimental and numerical verifications.

2. Theory and design

Fig. 1 shows the schematic of the electrostatically tunable microactuator using a curved comb-finger-width design. The control voltage, V_c, controls the resonant frequency of the mechanical microactuator. When the ac and dc voltages ($V_d + V_a \sin \omega t$) are applied to the conventional comb structure [11], the suspended microstructure is actuated by the sinusoidal force due to the applied voltage in the lateral direction. As shown in Fig. 2, a tuning comb structure consists of pairs of curved shape, stationary fingers and straight shape, movable fingers. The straight-shape fingers are placed on the movable structure in order to reduce the inertia of the movable structure. The profile of the stationary finger is designed to generate a constant electrostatic stiffness or linear electrostatic force that is independent of the displacement, x, under a control voltage, V_c. The symbols l_0, l, x, s_0, s, and s_1, are the length of the straight portion of the stationary finger, the length of the curved comb-finger-width portion of the stationary finger, the displacement of the movable finger, the initial space between the stationary and fixed fingers, the gap between the tip of the movable finger and the stationary finger at position x, and the final space between the stationary and fixed fingers, respectively.

Fig. 3 shows the infinitesimal stationary and movable finger surfaces, taken from Fig. 2, for theoretical derivation in resonant frequency and the effective electrostatic stiffness as a function of the control voltage. Under a control voltage V_c in Fig. 2, the stored energy U and the electrostatic force F_e on the movable finger are expressed as [12]

$$U = \frac{1}{2} C V_c^2 \tag{1}$$

$$F_e = \frac{\partial U}{\partial x} = \frac{1}{2} \frac{\partial C}{\partial x} V_c^2 \tag{2}$$

where C is the capacitance between the stationary and movable fingers. When the movable finger moves rightward by a displacement dx, the newly overlapped area in Fig. 3 provides the increase in the capacitance for small θ:

$$dC = \frac{\varepsilon \, dA}{s} = \frac{\varepsilon t \, dx}{s} \tag{3}$$

where dC, ε, dA, s, and t are the increase in the capacitance, the permitivity of air, the area increase corresponding to dx, the gap between the movable finger and the stationary finger at position x that will be derived below, and the thickness of the comb finger, respectively. The derivative of the capacitance is obtained from Eq. (3) as follows

$$\frac{dC}{dx} = \frac{\varepsilon t}{s} \tag{4}$$

It is noted from Eqs. (2) and (4) that dC/dx can be in the form of $ax+b$ to generate a force under a constant control voltage that is proportional to the displacement of the movable finger. Therefore, the profile, s, of the stationary comb finger from Eq. (4) is

$$s = \frac{\varepsilon t}{ax + b} \tag{5}$$

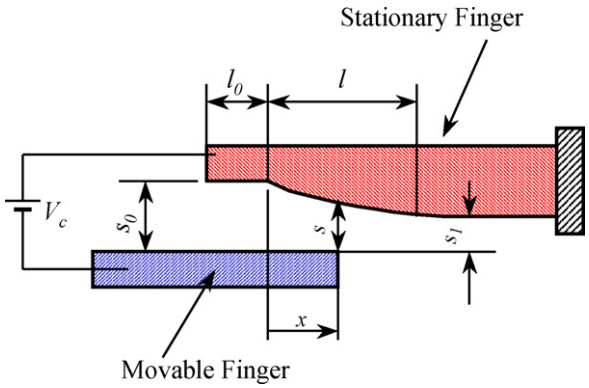

Fig. 2. A tuning comb structure showing curved, stationary finger and straight movable finger design: profile of the stationary finger is designed to generate a constant electrostatic stiffness independent of the displacement, x, under a control voltage, V_c.

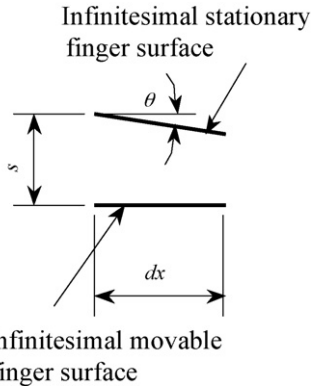

Fig. 3. Infinitesimal stationary and movable finger surfaces for derivation of stationary finger profile: s is space between the stationary and movable fingers at x in Fig. 2.

The following boundary conditions are used to obtain the constants a and b:

$$\text{at } x = 0, \quad \frac{\partial F_e}{\partial x} = 0 \text{ or } \frac{\partial C}{\partial x} = 0 \text{ and } s = s_0 \tag{6}$$

$$\text{at } x = l, \quad \frac{\partial F_e}{\partial x} = 0 \text{ or } \frac{\partial C}{\partial x} = 0 \text{ and } s = s_1 \tag{7}$$

Substituting Eqs. (6) and (7) into Eqs. (4) and (5), we can obtain the constants a and b as follows

$$a = \frac{1}{l}\left(\frac{\varepsilon t}{s_1} - \frac{\varepsilon t}{s_0}\right) \tag{8}$$

$$b = \frac{\varepsilon t}{s_0} \tag{9}$$

From Eqs. (5), (8) and (9), the s profile is derived as

$$s = s_0 \frac{1}{(s_0/s_1 - 1)(x/l) + 1} \tag{10}$$

Fig. 4 shows the theoretical s profile, calculated by using geometry of $s_0 = 4\,\mu m$, $s_1 = 2\,\mu m$, and $l = 10\,\mu m$ and it is found that s decreases when x increases to generate a linear electrostatic force (i.e. constant electrostatic stiffness) under a constant control voltage. The theoretical electrostatic force on the movable finger (Fig. 2) is obtained from Eqs. (2), (4) and (10)

$$F_e = \frac{1}{2}\frac{\partial C}{\partial x}V_c^2 = \frac{1}{2}\frac{\varepsilon t}{s_0}\left(\left(\frac{s_0}{s_1} - 1\right)\frac{x}{l} + 1\right)V_c^2 \tag{11}$$

Derivatives of Eq. (11) with respect to x provides the negative electrostatic stiffness k_e, due to the electrostatic attractive force of the movable and stationary fingers:

$$k_e = \frac{\partial F_e}{\partial x} = \frac{1}{2}\frac{\varepsilon t}{s_0 l}\left(\frac{s_0}{s_1} - 1\right)V_c^2 = \frac{F_e)_1 - F_e)_0}{l} \tag{12}$$

$$F_e)_0 = \frac{1}{2}\frac{\varepsilon t}{s_0}V_c^2 \tag{13}$$

$$F_e)_1 = \frac{1}{2}\frac{\varepsilon t}{s_1}V_c^2 \tag{14}$$

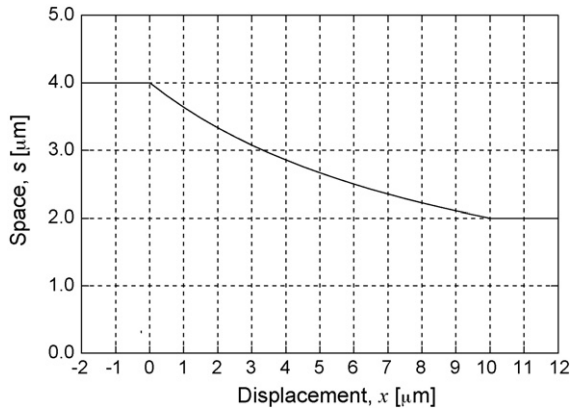

Fig. 4. Theoretical space profile is calculated by using geometry of $s_0 = 4\,\mu m$, $s_1 = 2\,\mu m$, and $l = 10\,\mu m$. It is observed that the profile decreases with x to generate a constant electrostatic force under a constant control voltage.

where $F_e)_0$ and $F_e)_1$ are the electrostatic forces at $x = 0$ and l in Fig. 2, respectively. Eq. (12) shows that the electrostatic stiffness equals to the force gradient between $x = 0$ and l and also implies that the effective electrostatic stiffness is linearly proportional to the square of the control voltage, V_c.

In order to obtain higher tuning capability, many pairs of tuning combs are preferred. Electrostatic tuning force of the tunable microactuator with N pairs of tuning combs is $2N$ times F_e of Eq. (11) because two basic structures of Fig. 2 constitute a pair of tuning comb:

$$F_{eN} = 2NF_e = N\frac{\varepsilon t}{s_0}\left(\left(\frac{s_0}{s_1} - 1\right)\frac{x}{l} + 1\right)V_c^2 \tag{15}$$

Similarly, the electrostatic stiffness of a tunable microactuator with N pairs of tuning comb fingers is obtained as follows

$$k_{eN} = 2Nk_e = N\frac{\varepsilon t}{s_0 l}\left(\frac{s_0}{s_1} - 1\right)V_c^2 = \gamma V_c^2 \tag{16}$$

$$\gamma = N\frac{\varepsilon t}{s_0 l}\left(\frac{s_0}{s_1} - 1\right) \tag{17}$$

where γ is a function of geometry of the microactuator shown in Figs. 1 and 2 and then can be defined as the electrostatic stiffness coefficient of the tunable comb-shape microactuator. It is noted that the electrostatic stiffness k_{eN} is a negative stiffness due to inherent electrostatic attractive force while positive electrostatic stiffness was demonstrated by using a laterally driven electrostatic repulsive force microactuator [13]. The effective stiffness, k_{eff}, and resonant frequency, f_r, of the microactuator under a constant control voltage, V_c, are then derived as follows

$$k_{eff} = k_s - \gamma V_c^2 \tag{18}$$

$$f_r = \frac{1}{2\pi}\sqrt{\frac{k_{eff}}{m}} = f_0\sqrt{1 - \frac{\gamma V_c^2}{k_s}} \tag{19}$$

$$f_0 = \frac{1}{2\pi}\sqrt{\frac{k_s}{m}} \tag{20}$$

where m, k_s and f_0 are the mass of the movable structure, the stiffness of the microactuator in the lateral direction and the resonant frequency at $V_c = 0\,V$, respectively. It is clear from Eqs. (18) and (19) that the effective stiffness and resonant frequency can be adjusted by changing the control voltage independent of the displacement of the movable finger. Table 1 summarizes the parameters and calculated results of the designed tunable microactuator with 186 pairs of comb fingers to generate higher electrostatic stiffness coefficient (γ).

Finite element analysis (FEA) is conducted using MAXWELL for the two-dimensional electrostatic force analysis. Fig. 5 depicts equipotential lines around movable and stationary fingers from the MAXWELL simulation using the geometry of $s_0 = 4\,\mu m$, $s_1 = 2\,\mu m$, and $l = 10\,\mu m$. Fig. 6 compares the theoretical electrostatic force of Eq. (11) and the simulated electrostatic force per unit thickness when a pair of tuning comb with the geometry of Table 1 is used. Fig. 6 shows that the simple expression of Eq. (15) predicts linear relationship between the electrostatic force and movement, x, in

Table 1
Designed parameters of the tunable microactuator

Mass, m ($\times 10^{-10}$ kg)	1.85
Stiffness,[a] k_s (N/m)	2.64
Resonant frequency, f_0 (kHz)	19
Number of fingers, N	186
Thickness, t (μm)	2
Length of the varied comb-width, l (μm)	10
Length of the straight portion of the stationary finger, l_0 (μm)	5
Initial space between the stationary and fixed fingers, s_0 (μm)	4
Final space between the stationary and fixed fingers, s_1 (μm)	2
Electrostatic stiffness coefficient,[b] γ_{th} ($\times 10^{-5}$ N/mV^2)	8.22

[a] Based on Young's modulus of 111.7 GPa from a polysilicon test structure.
[b] Based on Eq. (17).

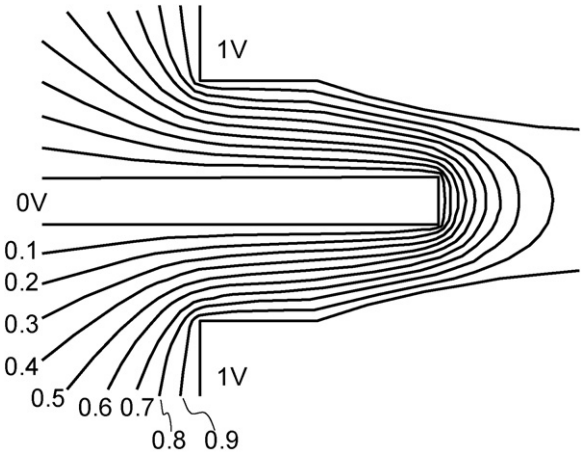

Fig. 5. Equipotential lines around movable and stationary fingers from MAXWELL simulation: $s_0 = 4$ μm, $s_1 = 2$ μm, and $l = 10$ μm.

the range of $x = 0$–10 μm and that the electrostatic force keeps at constant values for the range of $x \leq 0$ μm and $x \geq 10$ μm. The simulated force in Fig. 6 follows the theoretical force from Eq. (15) for $x = 2$–8 μm but the simulated electrostatic force (proportional to dC/dx) is higher around the $x = 0$ μm region and lower near the $x = 10$ μm region. These discrepancies are probably due to use of simplified boundary conditions of Eqs. (6) and (7). The theoretical and simulated electrostatic stiffness coefficients from $x = 2$ μm to 8 μm are estimated as

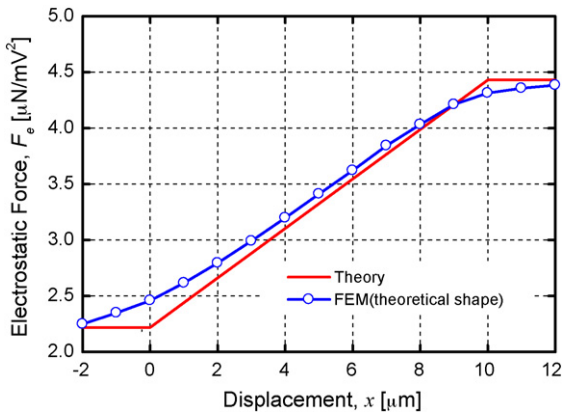

Fig. 6. Theoretical and simulated electrostatic forces per unit thickness for the movable finger in Fig. 2: $s_0 = 4$ μm, $s_1 = 2$ μm, and $l = 10$ μm.

0.221 N/(m^2 V^2) and 0.212 N/(m^2 V^2) per unit thickness around $x = 5$ μm from the slopes of Fig. 6, respectively. It is noted that the electrostatic stiffness from Eq. (16) is 4.2% higher than that from the finite element analysis. Under an arbitrary control voltage, Eqs. (15), (16), and (18) can be used in the design process to provide a linear response in electrostatic force with respect to displacement and to achieve a constant effective stiffness independent of position of comb. As a result, the resonant frequency can be actively adjusted as a function of the effective stiffness by the control voltage.

3. Fabrication, results and discussions

Tunable microactuators have been fabricated by the standard surface micromachining process [14]. Fig. 7 shows the SEM photograph of one released microactuator where the total size is 480 μm × 840 μm with 186 tuning comb-pairs for the active electrostatic stiffness control. Fig. 8 shows top views of the stationary and movable fingers. Sizes of s_0, s_1, l are designed as

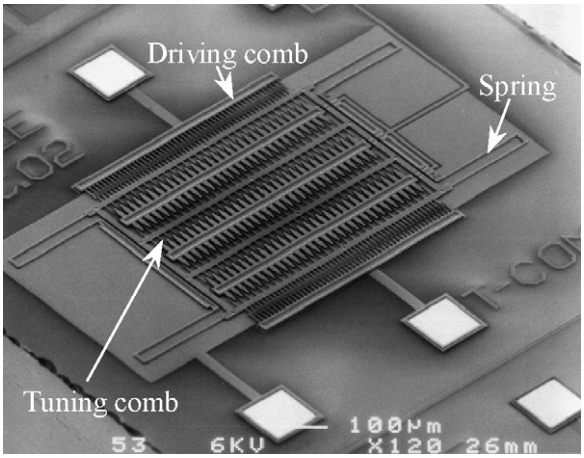

Fig. 7. SEM photograph of the fabricated tunable microactuator, made of 2 μm-thick polysilicon with a total size of 460 μm × 840 μm and 186 pairs of tuning combs are used to generate the tuning force.

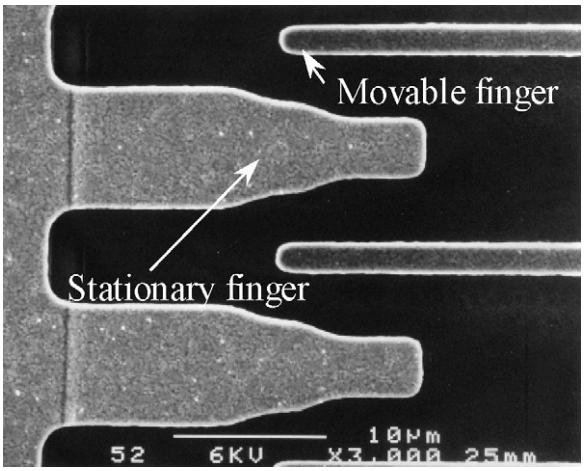

Fig. 8. Top view of the comb fingers: s_0, s_1, l are designed as 4 μm, 2 μm, and 10 μm, respectively. The shape of the stationary finger is slightly different from the theoretical curve of Eq. (10) due to lithographic errors.

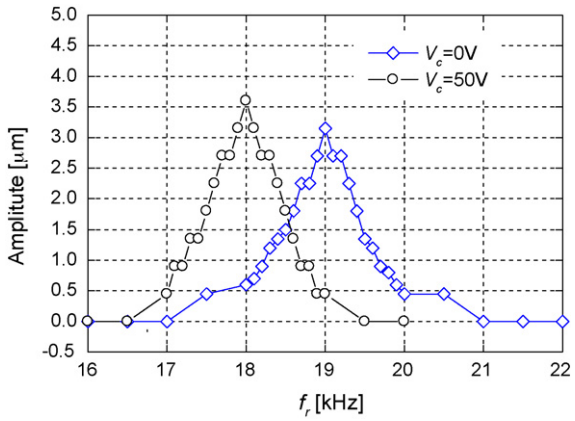

Fig. 9. Dynamic response of the microactuator for control voltages of 0 V and 50 V.

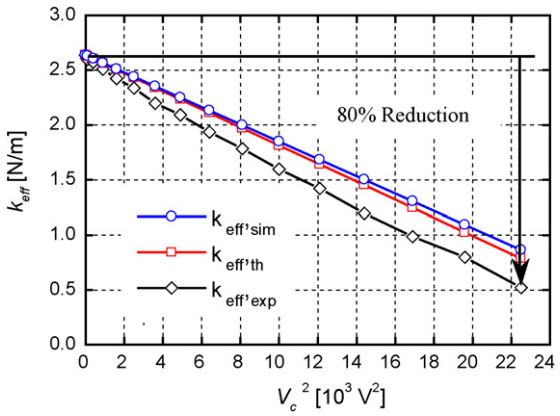

Fig. 11. Effective stiffness derived from Fig. 10 from 0 V to 150 V. The measured electrostatic stiffness coefficient, γ, is estimated as 9.4×10^{-5} N/mV^2.

4 μm, 2 μm, and 10 μm, respectively. In order to achieve higher resonant frequency, the stationary finger is designed by using Eq. (10). The fabricated profile is slightly different from the theoretical shape of Eq. (10) due to lithographic errors.

The fabricated tunable microactuator was optically observed to actuate under atmospheric pressure with a 10 Vpp ac driving voltage and a 40 V dc bias voltage in Fig. 1. The control voltage is adjusted from 0 V to 50 V while the microstructures are actuated. Fig. 9 shows the frequency response of the fabricated microactuator electrostatically tuned by the control voltage of 0 V and 50 V, respectively. The resonant frequency of 19.0 kHz at $V = 0$ V is reduced to 18.0 kHz when the control voltage is increased from 0 V to 50 V. This frequency reduction phenomenon is expected from the theoretical derivation (Eq. (19)) that the resonant frequency is a function of the electrostatic stiffness, the control voltage, and the mechanical stiffness. It is noted from Fig. 9 that the peak resonant amplitude at $V_c = 50$ V is greater than that at $V_c = 0$ V because higher control voltage provides lower effective stiffness from Eq. (18). Fig. 10 compares the theoretical, simulated and experimental resonant frequencies for the control voltage in the range of 0–150 V. The theoretical resonant frequency is calculated by Eq. (19) and the electrostatic stiffness coefficient of 7.88×10^{-5} N/(m V^2) is derived from Fig. 6 for the prototype structure. It is observed that the theoretical, simulated and measured resonant frequencies decrease from the original frequency of 19.0–10.38 kHz, 10.88 kHz, and 8.45 kHz, respectively when the control voltage varies from 0 V to 150 V. The frequency reductions in the theoretical, simulated and measured resonant frequencies are estimated as 45.4%, 42.7%, and 55.5% of the original frequency, respectively. The measured resonant frequency reduction is a bit larger than the theoretical and simulated ones and one reason of this discrepancy could come from lithographic errors as illustrated in Fig. 8. If the discrepancy is from the lithographic errors, the designed profile on the lithographic mask may be compensated to reduce the lithographic errors.

Fig. 11 shows the effective stiffness, k_{eff}, derived from the theoretical, simulated, and experimental results of Fig. 10. All graphs in Fig. 11 are linearly proportional to voltage squared. The experimental effective stiffness reduces by 80% from the initial stiffness of 2.64 N/m. From the slope of the data in Fig. 11, the theoretical, simulated, and experimental electrostatic stiffness coefficients, γ, are estimated as 8.22×10^{-5} N/mV^2, 7.88×10^{-5} N/mV^2, and 9.4×10^{-5} N/mV^2, respectively.

FEA using MAXWELL is conducted using the theoretical finger shape profile (Eq. (10)) and the fabricated one that is measured from enlarged SEM photograph. Fig. 12 shows the simulated electrostatic force per unit thickness for the theoretical and fabricated finger shapes and it shows that electrostatic stiffness (i.e. the slope of the force curve) from the fabricated

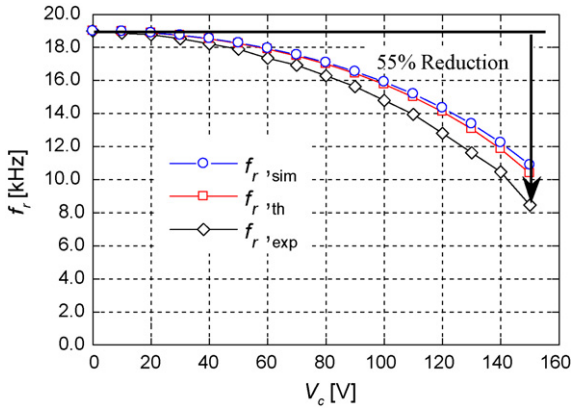

Fig. 10. Resonant frequency tuning under various control voltage.

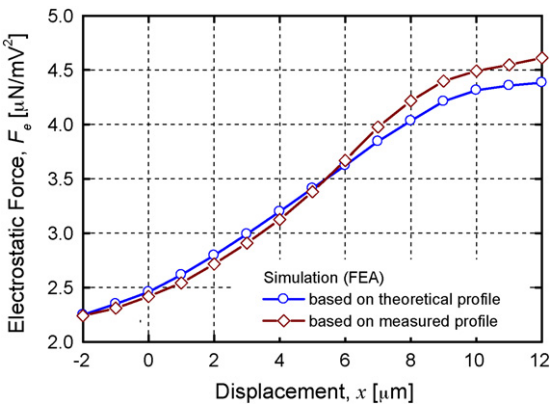

Fig. 12. Simulated electrostatic forces per unit thickness on the movable finger in Fig. 2 of both theoretical and fabricated profiles.

Table 2
Electrostatic stiffness coefficient of the microactuator[a]

Theory, γ_{th} ($\times 10^{-5}$ N/mV^2)	8.22
FEA using theoretical shape profile, γ_{sim} ($\times 10^{-5}$ N/mV^2)	7.88
FEA using fabricated shape profile, γ_{sim1} ($\times 10^{-4}$ N/mV^2)	1.01
Experiment, γ_{exp} ($\times 10^{-5}$ N/mV^2)	9.40

[a] Data in Table 1 are used.

finger shape around $x = 5\,\mu$m is higher than that from the theoretical finger shape. The electrostatic stiffness coefficient, γ, from the experiment and simulation using the fabricated profile are estimated as 9.40×10^{-5} N/mV^2 and 1.01×10^{-4} N/mV^2, respectively. Table 2 summarizes the electrostatic stiffness coefficients, γ, from theory, simulation with analytical profile, simulation with fabricated profile and experimental results, respectively. The simulation result with fabricated profile seems to have the closest one to the measurement result. These results demonstrate that closed-form equations for effective stiffness and resonant frequency presented in this paper can be used for a first-order approximation for frequency- and stiffness-tunable microdevices based on the curved comb-finger-width designs with possible applications for resonant-based devices including microelectromechanical filters [15].

4. Conclusions

We have established a closed-form, curved comb finger profile to obtain a constant electrostatic stiffness when the movable finger engages the stationary finger. The theoretical comb-finger-width profile provides a constant electrostatic stiffness, independent of the position or displacement of the combs. A tunable microactuator, having 186 comb pairs of the varied comb-finger-width profile, was designed and fabricated by a standard surface micromachining process. Experimentally, its resonant frequency has been reduced by 55% from the initial frequency of 19 kHz under a bias voltage of 150 V and the reduction is linearly proportional to the square of the control voltage as expected. The electrostatic stiffness coefficient, γ, representing a capability of the stiffness and resonant frequency adjustment are estimated as 8.22×10^{-5} N/mV^2 from the theory and 9.40×10^{-5} N/mV^2 from experiment. As such, the closed-form approach of the comb-finger profile can be applied to other comb-shape actuators for frequency control as well as constructing linear electrostatic stiffness with respect to displacement.

References

[1] H. Xu, E. Gao, Q.Y. Ma, Active tuning of high frequency resonators and filters, IEEE Trans. Appl. Supercond. 11 (1) (2001) 353–356.
[2] J. Soderkvist, Design of a solid-state gyroscopic sensor made of quartz, Sens. Actuators A 21 (1990) 293–296.
[3] A. Cheshmehdoost, S. Stroumbouhs, B. O'Connor, B.E. Jones, Dynamic characteristics of a resonating force transducer, Sens. Actuators A 41–42 (1994) 74–77.
[4] A. Cheshmehdoost, B.E. Jones, Design and performance characteristics of an integrated high-capacity DETF-based force sensor, Sens. Actuators A 52 (1996) 99–102.
[5] K. Bang Lee, Y.-H. Cho, A triangular electrostatic comb array for micromechanical resonant frequency tuning, Sens. Actuators A 70 (1998) 112–117.
[6] M. Chiao, L. Lin, Post-packaging frequency tuning of microresonators by pulsed laser deposition, J. Micromech. Microeng. 14 (12) (2004) 1742–1748.
[7] R.R.A. Syms, Electrothermal frequency tuning of folded and coupled vibrating micromechanical resonators, J. Microelectromech. Syst. 7 (2) (1998) 164–171.
[8] T. Remtema, L. Lin, Active frequency tuning for microresonators by localized thermal stressing effects, Sens. Actuators A 91 (2001) 326–332.
[9] W. Ye, S. Mukherjee, N.C. MacDonald, Optimal shape design of an electrostatic comb drive in microelectromechanical systems, J. Microelectromech. Syst. 7 (1) (1998) 16–26.
[10] B.D. Jensen, S. Mutlu, S. Miller, K. Kurabayashi, J.J. Allen, Shaped comb fingers for tailored electromechanical restoring force, J. Microelectromech. Syst. 12 (3) (2003) 373–383.
[11] W.C. Tang, C.T.-C. Nguyen, R.T. Howe, Laterally driven polysilicon resonant microstructures, Sens. Actuators A 20 (1989) 25–32.
[12] H.H. Woodson, J.R. Melcher, Electromechanical Dynamics, John Wiley & Sons Inc., 1968.
[13] K.B. Lee, Y.-H. Cho, Laterally driven electrostatic repulsive-force microactuators using asymmetric field distribution, J. Microelectromech. Syst. 10 (1) (2001) 128–136.
[14] J. Carter, A. Cowen, B. Hardy, R. Mahadevan, M. Stonefield, S. Wilcenski, PolyMUMPs Design Hand Book, Revision 11.0, MEMSCAP Inc., 2006, http://www.memsrus.com.
[15] R.T. Liwei Lin, A.P. Howe, Pisano, Microelectromechanical filters for signal processing, J. Microelectromech. Syst. 7 (3) (1998) 286–294.

Biographies

Ki Bang Lee is the director of KB Lab in Singapore, a research laboratory that focuses on cutting-edge technologies for bioscience, healthcare and MEMS. He received the B.S., M.S., and Ph.D. degrees, all in mechanical engineering, from Hanyang University, Seoul, Korea, and the Korea Advanced Institute of Science and Technology (KAIST), Korea, in 1985, 1987, and 2000, respectively. He worked for Samsung Advanced Institute of Technology (SAIT), Yonginsi, Korea during 1987–2000, holding the last position of principal research scientist, and then was a research specialist of the Berkeley Sensors and Actuator Center (BSAC) at the University of California at Berkeley during 2000–2004. As a principal research scientist, he worked with Institute of Bioengineering and Nanotechnology (IBN) in Singapore during 2004–2005. Since 2005, he has worked as a director with KB Lab on urine-(biofluid-)activated paper battery for biosystems and self-activated healthcare test kits/biochips that can diagnose diseases or check up our health by using biofluids. His research interests include power generation from biofluid, self-activated biosystems on a chip, labs-on-a-chip, and theory and fabrication of MEMS, NEMS and bioMEMS.

Liwei Lin joined UC-Berkeley in 1999 and is now chancellor's professor at the Mechanical Engineering Department and co-director at the Berkeley Sensor and Actuator Center. He received his B.S. (1986) in power mechanical engineering from National Tsing Hua University, M.S. (1991) and Ph.D. (1993) in Mechanical Engineering from the University of California at Berkeley. He was an associate professor in the Institute of Applied Mechanics, National Taiwan University, Taiwan (1994–1996) and an assistant professor in Mechanical Engineering Department, University of Michigan (1996–1999). His research interests are in design, modeling and fabrication of micro/nano-structures, micro/nano-sensors and micro/nano-actuators as well as mechanical issues in micro/nano-systems including heat transfer, solid/fluid mechanics and dynamics. Dr. Lin is the recipient of the 1998 NSF CAREER Award for research in MEMS Packaging and the 1999 ASME Journal of Heat Transfer best paper award for his work on micro-scale bubble formation. Currently, he serves as a subject editor for the IEEE/ASME Journal of Microelectromechanical Systems and the North and South America Editor of Sensors and Actuators—A Physical. He led the effort to establish the MEMS division in ASME and served as the founding Chairman of the Executive Committee from 2004 to 2005. He is an ASME Fellow and has 10 issued US patents in the area of MEMS.

Young-Ho Cho received the B.S. degree *summa cum laude* from Yeungnam University, Daegu, Korea, in 1980; the M.S. degree from the Korea Advanced Institute of Science and Technology (KAIST), Seoul, Korea, in 1982; and the Ph.D. degree from the University of California at Berkeley for his electrostatic actuator and crab-leg microflexure research completed in December 1990. Previously, he was a research scientist (1882–1986) of CAD/CAM Research Laboratory, Korea Institute of Science and Technology (KIST), Seoul, Korea. He also worked as a post-graduate researcher (1987–1990) and a post-doctoral research associate (1991) of the Berkeley Sensor and Actuator Center (BSAC) at the University of California at Berkeley. In August 1991, Dr. Cho moved to KAIST, where he is currently a professor in the Departments of BioSystems & Mechanical Engineering as well as the director of Digital Nanolocomotion Center. Dr. Cho's research interests are focused on the nano/microelectromechanical systems with bio-inspired actuators and detectors for the manipulation and processing of non-electrical information carriers or substances in nano/micro-regime. In Korea, he served as the founding chair of MEMS Division in Korean Society of Mechanical Engineers, the chair of steering committee in Korea National MEMS Programs, and the committee member of National Nanotechnology Programs. Dr. Cho also served for International Technical Society as the general co-chair of IEEE MEMS Conference 2003, the committee member of IEEE Optical MEMS Conference, the committee member of Power MEMS Conference, and the chief delegate of the Republic of Korea in World Micromachine Summit. Dr. Cho is a member of IEEE and ASME.